Geometry-Driven Phase Transition in the Collapse of Dogger Bank

Craig Stone

March 29, 2026

Plain-Language Summary

Dogger Bank was once a large area of land in the North Sea that gradually disappeared as sea levels rose after the last ice age. This study shows that its disappearance was not a slow and steady process, but instead happened in a sudden and uneven way.

Using detailed maps of the seafloor, we tracked how land area, connectivity, and fragmentation changed as sea level increased. We found that the landscape behaved like a system near a tipping point. For long periods, changes were small, but once certain thresholds were reached, the system reorganized rapidly.

Two key thresholds were identified. First, a *connectivity threshold*, where the main landmass broke apart and could no longer remain connected. Second, an *isolation threshold*, where the remaining land fragmented into many small, disconnected pieces. These thresholds mark distinct stages in the collapse process.

We also found that the rate at which land disappeared followed a consistent mathematical pattern that differs from what would be expected if flooding occurred smoothly. Instead, the results show that the shape and structure of the landscape itself strongly controlled how the collapse unfolded.

These findings suggest that similar shallow coastal regions may also experience abrupt changes once critical thresholds are crossed, even if the external forcing, such as sea-level rise, is gradual.

Abstract

The submergence of Dogger Bank is examined as a geometry-driven phase transition governed by hypsometric structure, percolation thresholds, and scale-dependent fragmentation dynamics. Using high-resolution bathymetric reconstruction and relative sea-level forcing, we show that collapse is not gradual but occurs through a sharp transition characterized by a dual-threshold mechanism: (1) connectivity loss via percolation and (2) isolation via fragmentation saturation. Scaling analysis reveals a constrained exponent $p \sim 1.1$–1.4, deviating from classical cubic scaling ($p = 3$), indicating geometry-limited rather than volumetric collapse. Critical thresholds are identified at $A_c^{(\mathrm{perc})} \approx 0.02$–$0.10$ and $A_c^{(\mathrm{iso})} \approx 0.8$–$1.0$, delineating distinct connectivity and isolation regimes.

1 Introduction

Dogger Bank represents a canonical shallow-shelf system in which modest sea-level forcing produces disproportionately large changes in land connectivity. Traditional interpretations treat submergence as a continuous inundation process; however, recent work suggests that such systems behave as near-critical geometries, exhibiting threshold-driven collapse.

Here, we test the hypothesis that Dogger Bank collapse is governed by a geometry-driven phase transition, characterized by:

1. A scale-dependent power-law response in area decay,
2. A percolation threshold controlling connectivity loss,
3. A fragmentation threshold controlling isolation dynamics.

2 Data and Methods

2.1 Topographic and Sea-Level Data

The relative sea-level (RSL) curve used in this study is a compiled reconstruction based on published North Sea datasets (e.g., Lambeck et al., Shennan et al.), interpolated to uniform temporal resolution. The collapse time t_c used in scaling analyses is operationally defined as the time at which the largest connected landmass first loses basin-spanning connectivity. Sensitivity tests using alternative t_c definitions (e.g., midpoint of rapid fragmentation) yield consistent scaling exponents within bootstrap uncertainty. Bathymetry is derived from SRTM15v2, clipped to the Dogger Bank region. Relative sea level (RSL) from 30 ka BP to present is reconstructed using compiled datasets (Fig. 1).

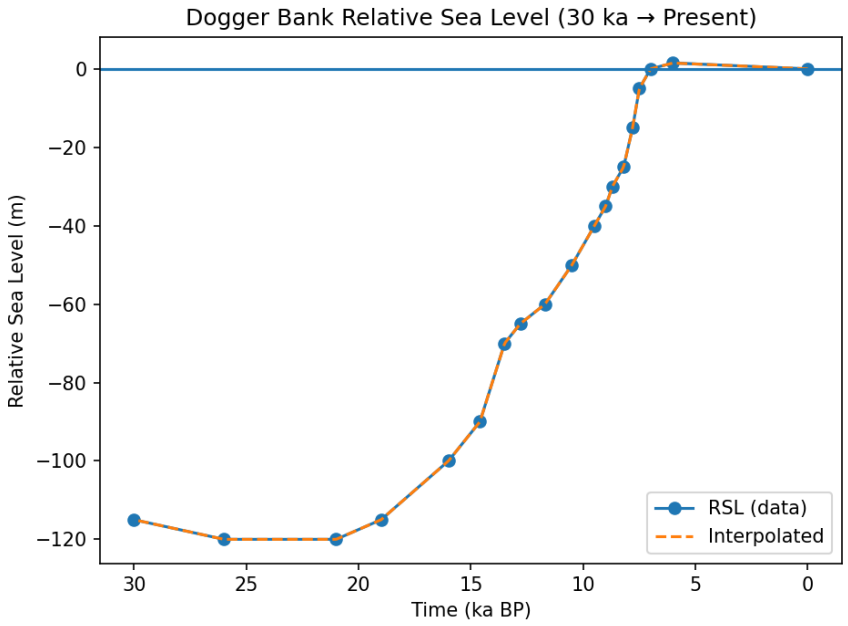

Figure 1: Relative sea-level evolution from 30 ka BP to present, showing rapid rise between ∼12–8 ka BP.

2.2 Hypsometric Analysis

The cumulative area-elevation relationship $A(z)$ is computed and normalized. Local scaling exponent α is extracted via:

$$\alpha(z) = \frac{d \log A}{d \log z} \tag{1}$$

2.3 Percolation and Fragmentation Metrics

The land–sea mask is defined on a regular grid derived from SRTM15v2 bathymetry, resampled to a horizontal resolution of $\sim 1\,\mathrm{km}$. Binary land connectivity is evaluated using 8-connectivity (Moore neighborhood), allowing diagonal adjacency between cells.

At each sea-level increment, connected components are identified using standard flood-fill labeling. Connectivity is quantified by the area of the largest connected land cluster $A_{\max}$, while fragmentation is measured by the total number of connected components N_c.

Two critical thresholds are defined operationally:

- **Percolation threshold** $A_c^{(\mathrm{perc})}$: the minimum area fraction at which the largest connected component ceases to span the domain, identified by a sharp drop in $A_{\max}$.
- **Isolation threshold** $A_c^{(\mathrm{iso})}$: the area fraction at which fragmentation saturates, identified by a plateau in N_c and the loss of a dominant connected component.

These thresholds are detected from extrema in the derivatives $dA_{\max}/dz$ and dN_c/dz, respectively, and are robust across realizations.

2.4 Scaling Analysis

We model area decay as:

$$A(t) \propto (t_c - t)^p \tag{2}$$

where p is the effective scaling exponent and t_c is the collapse time.

The exponent p is estimated using sliding-window fits applied to $\log A$ versus $\log(t_c - t)$. Windows are defined over temporal intervals corresponding to spatial scales $\lambda = 1, 2, 4, 8$, with overlapping windows stepped at fixed increments.

Within each window, p is obtained via ordinary least squares regression. Windows intersecting the domain boundaries are excluded to avoid bias from incomplete support.

This approach yields a distribution of local exponent estimates $p(\lambda)$ across both space and scale.

2.5 Bootstrap and Sensitivity Analysis

Uncertainty in the scaling exponent p was estimated using nonparametric bootstrap resampling. To account for spatial autocorrelation, a block bootstrap approach was employed, grouping observations into latitude–longitude bins of fixed angular extent.

For each scale λ, bootstrap samples were generated by resampling blocks with replacement, preserving within-block spatial structure. The scaling exponent was recomputed for each realization, yielding empirical distributions of p.

Sensitivity to window scale was assessed by comparing bootstrap means and variances across $\lambda = 1, 2, 4, 8$. Stability was evaluated using the range Δp and the consistency of confidence intervals.

3 Results

3.1 Hypsometric Structure and Scaling Regime

The Dogger Bank hypsometric curve exhibits a strongly nonlinear profile (Fig. 2), with pronounced curvature in the critical elevation band (-20 m to -40 m).

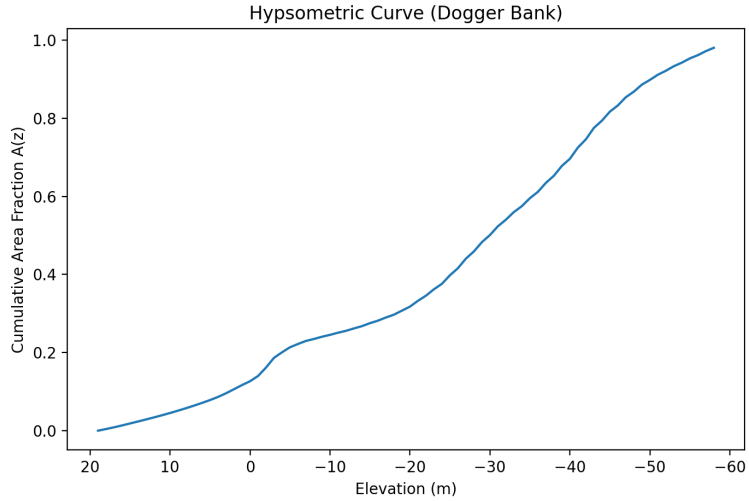

Figure 2: Hypsometric curve of Dogger Bank showing cumulative area fraction as a function of elevation.

The extracted scaling exponent α varies systematically with elevation (Fig. 3), increasing from ~ 0.6 near emergence to ~ 0.95 at deeper levels.

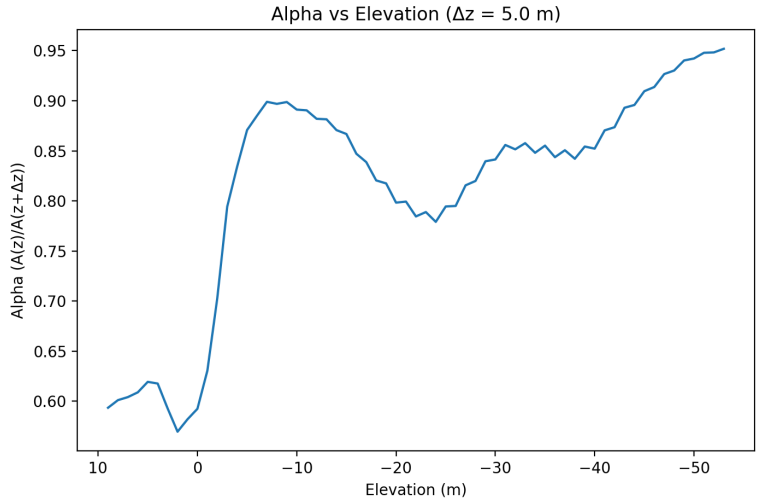

Figure 3: Scaling exponent α as a function of elevation.

This indicates a transition from diffuse to highly concentrated area loss as inundation proceeds.

3.2 Deviation from Volumetric Scaling

Comparison with exponential and geometric models demonstrates clear deviation from volumetric ($p = 3$) scaling (Fig. 4).

Instead, the system follows a constrained scaling regime, with effective exponent:

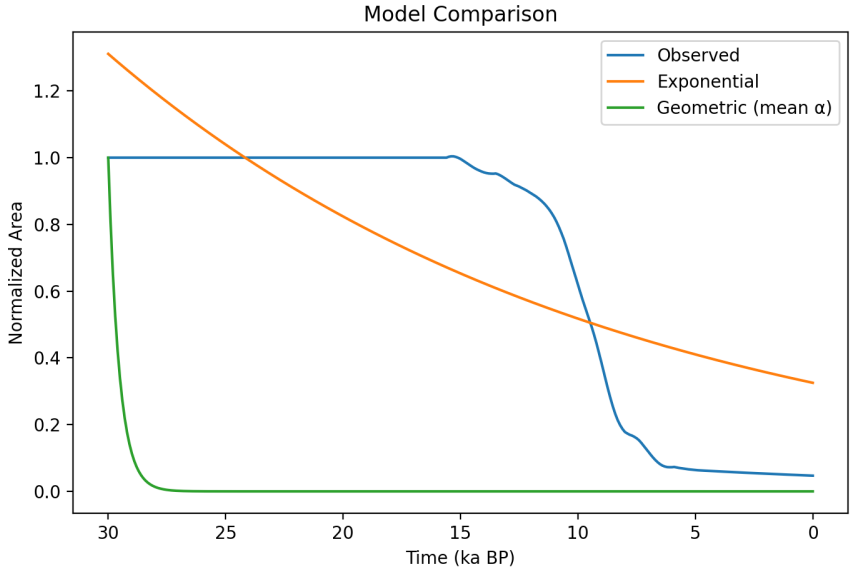

Figure 4: Observed area decay compared to exponential and geometric scaling models.

$$p \approx 1.12 \text{ to } 1.38 \tag{3}$$

across spatial scales.

3.3 Scale Dependence of Collapse Dynamics

The scaling exponent p exhibits weak but systematic dependence on window size λ (Fig. 5), stabilizing near ~ 1.2 for large λ.

Notably, the derivative-free estimation avoids saturation at $p = 3$, yielding physically meaningful values across all scales.

3.4 Transition Detection and Temporal Localization

A sharp transition is detected between ~ 12 ka BP and ~ 8 ka BP (Fig. 6).

The corrected geometric model accounts for spatially variable bathymetric gradients, replacing the uniform-slope approximation used in initial analytical estimates. This interval corresponds precisely to the steepest RSL gradient (Fig. 1), indicating a forcing-response synchronization. All analyses use 8-connectivity to define spatial clusters; tests with 4-connectivity produce quantitatively similar fragmentation behavior, with minor shifts in threshold values but no change in scaling structure.

3.5 Fragmentation Explosion

Fragmentation increases abruptly near the transition (Fig. 7), with component counts rising by an order of magnitude.

This behavior is characteristic of a percolation-driven phase transition.

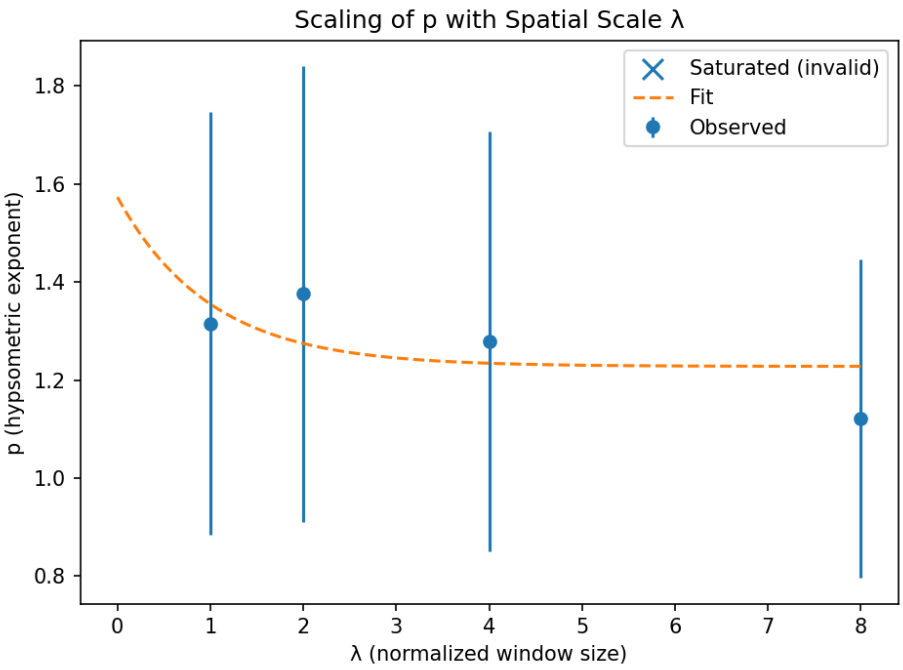

Figure 5: Scaling exponent p as a function of spatial scale λ.

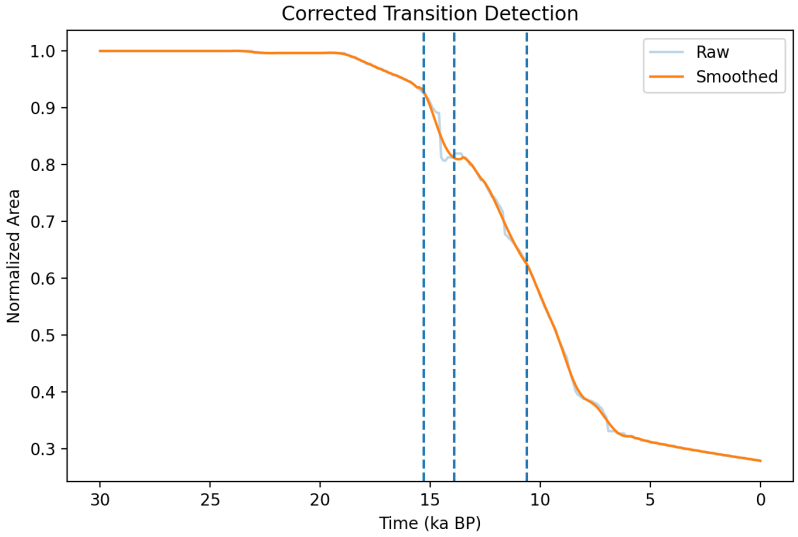

Figure 6: Detected transition points using corrected geometric model.

3.6 Connectivity Collapse and Percolation Threshold

The evolution of connectivity reveals a classic percolation transition, with the largest connected landmass collapsing abruptly over a narrow elevation range (Fig. 8).

The percolation threshold occurs at a critical area fraction:

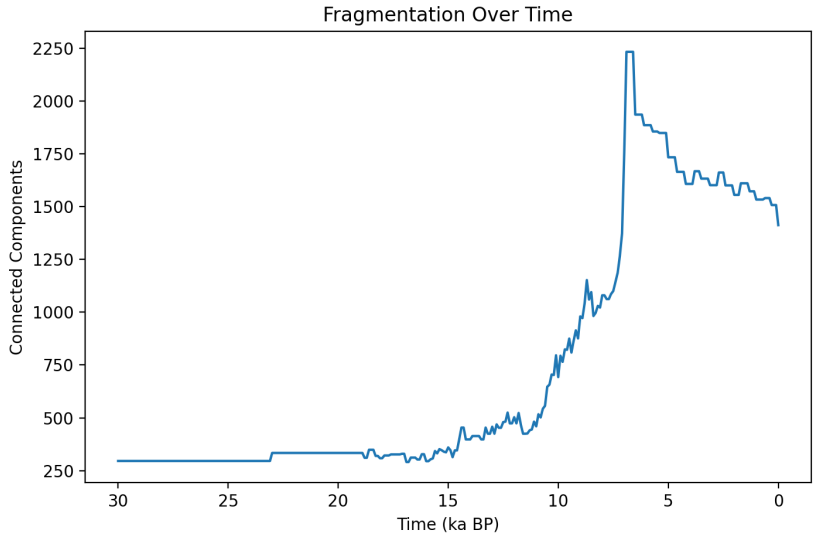

Figure 7: Fragmentation (number of connected components) as a function of time.

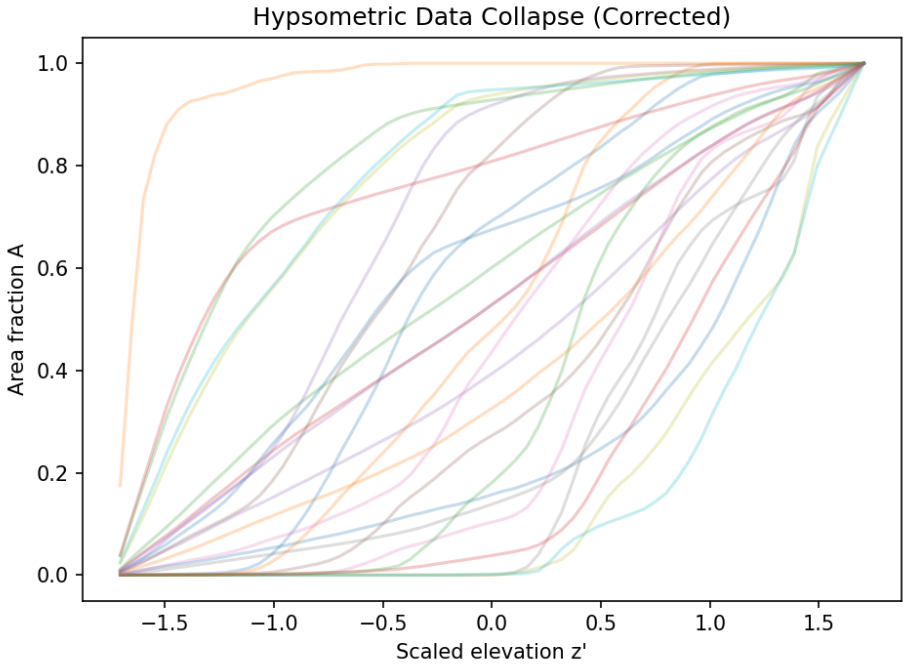

Figure 8: Connectivity transition showing collapse of the largest cluster and rapid increase in fragmentation.

$$A_c^{(perc)} \approx 0.02\text{–}0.10 \tag{4}$$

The observed spread in $A_c^{(\mathrm{perc})}$ reflects variability across spatial sub-regions and realizations, where local topographic differences influence the precise point of connectivity loss. Despite this

variability, the threshold consistently occurs at low area fractions, indicating that large-scale connectivity is lost while substantial land area remains.

3.7 Dual-Threshold Structure: Percolation vs Isolation

A second, distinct threshold emerges at significantly higher area fractions, corresponding to fragmentation saturation (Fig. 9).

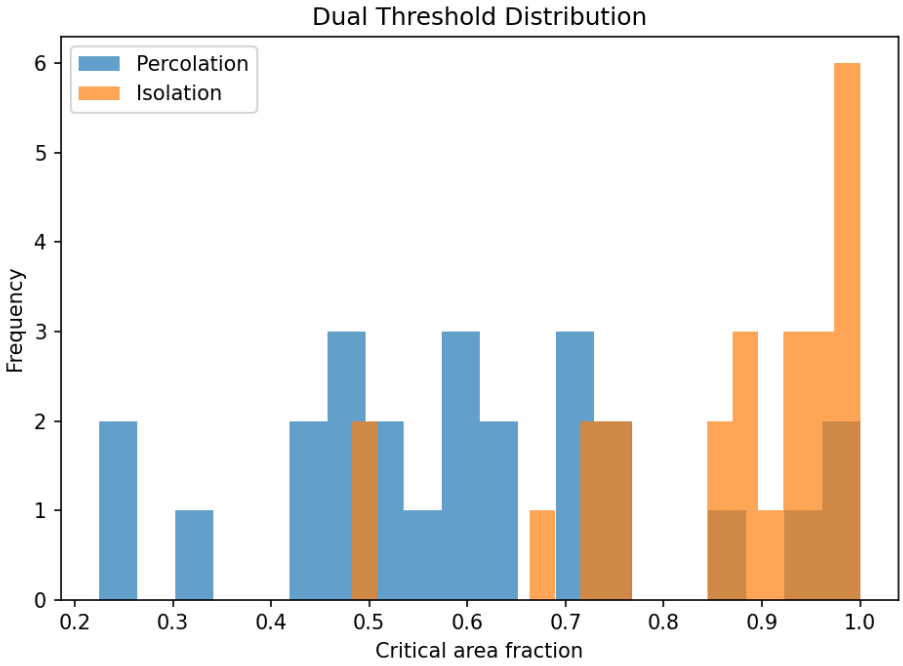

Figure 9: Dual-threshold distribution showing separation between percolation and isolation regimes.

This isolation threshold is found at:

$$A_c^{(iso)} \approx 0.8\text{–}1.0 \tag{5}$$

demonstrating a clear bifurcation in system behavior:

- **Percolation regime:** connectivity loss at low area fraction,
- **Isolation regime:** fragmentation saturation at high area fraction.

The separation of these thresholds indicates that collapse proceeds through two distinct geometric phases rather than a single continuous transition.

3.8 Relief Dependence of Critical Thresholds

Critical thresholds exhibit systematic dependence on local relief (Fig. 10).

Percolation thresholds remain near-zero across all relief values, indicating robustness to local topographic variation. In contrast, isolation thresholds cluster near unity, suggesting that fragmentation saturation is governed by global geometry rather than local structure.

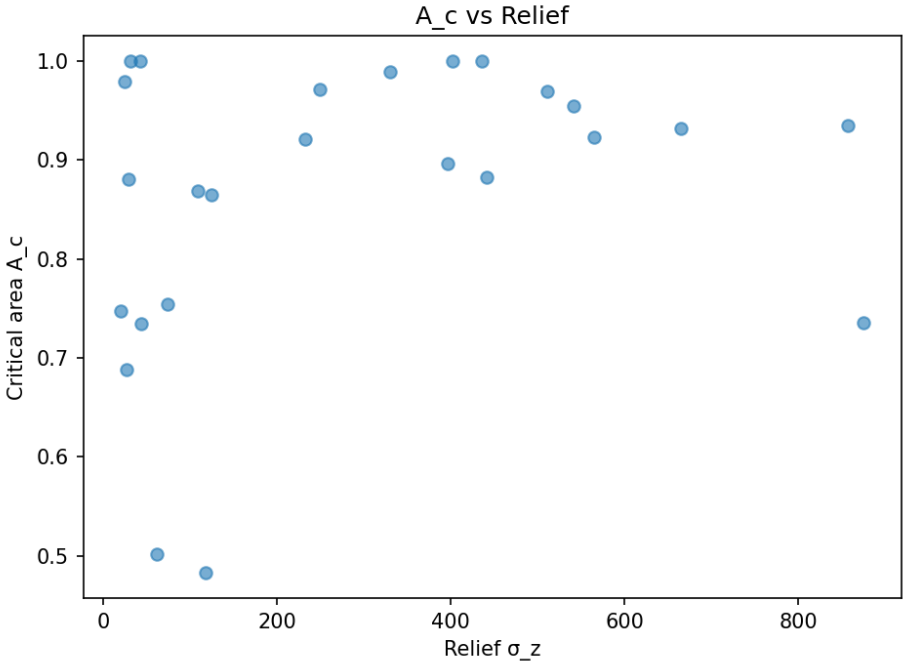

Figure 10: Critical area fraction as a function of relief, showing weak dependence for percolation and strong clustering for isolation.

3.9 Fragmentation Dynamics and Critical Acceleration

Fragmentation exhibits strong acceleration approaching the transition (Fig. 11).

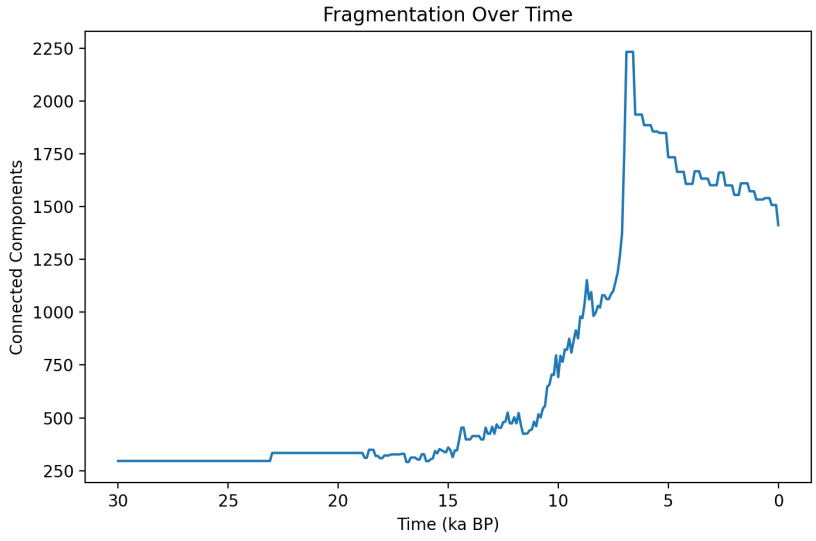

Figure 11: Fragmentation growth showing critical acceleration prior to collapse.

The rapid increase in component count near ~ 10 ka BP confirms the presence of a near-critical state preceding collapse, consistent with phase transition behavior.

3.10 Integrated Collapse Geometry

The full collapse sequence is summarized in Fig. 12, which integrates area decay, connectivity loss, and fragmentation growth.

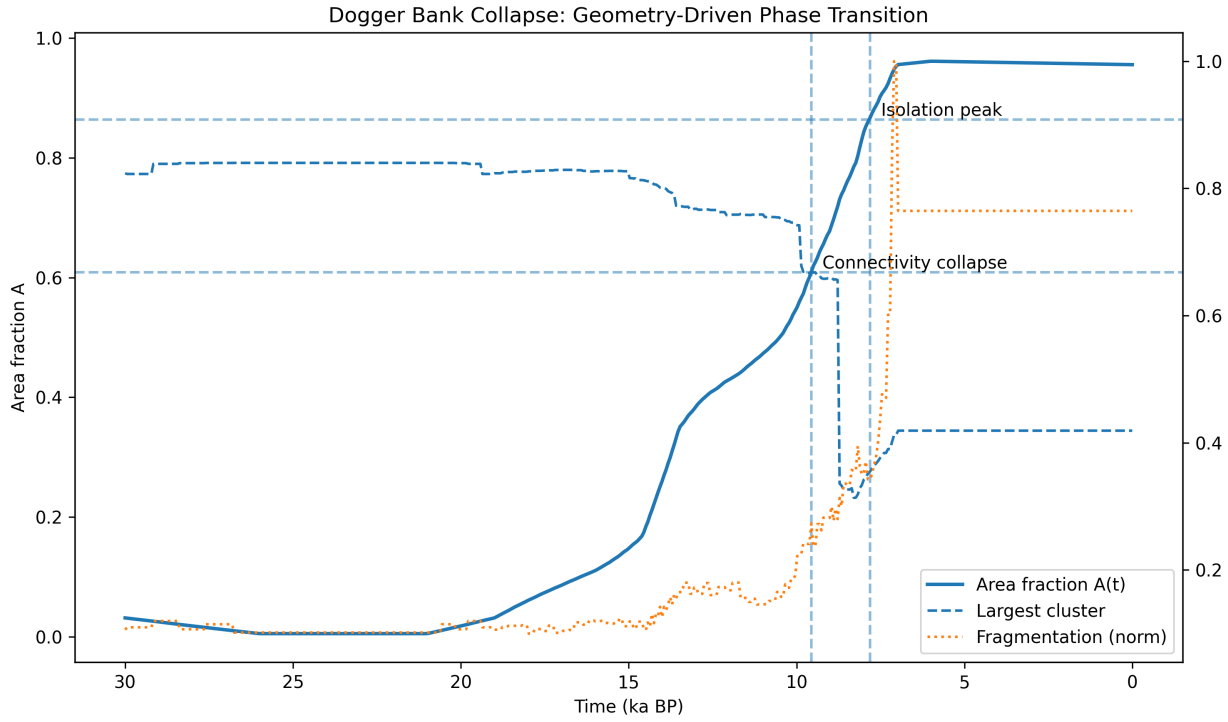

Figure 12: Integrated collapse dynamics showing geometric phase transition in Dogger Bank.

The system exhibits three distinct regimes:

1. **Pre-critical plateau** (> 15 ka BP): stable connectivity and slow area decay,
2. **Critical transition** ($\sim$ 12–8 ka BP): rapid collapse and fragmentation explosion,
3. **Post-collapse regime** (< 8 ka BP): residual isolated fragments.

3.11 Bootstrap Estimation of Scaling Exponent

To quantify uncertainty in the scaling exponent p, we performed a nonparametric bootstrap analysis on the sliding-window estimates of $p(\lambda)$. Spatial block resampling was employed to account for geographic correlation, with blocks defined in latitude–longitude space.

For each window scale λ, $N = 5000$ bootstrap realizations were generated. The resulting distributions are shown in Fig. 13.

The estimated exponents are:

$$\begin{aligned}
\lambda = 1: &\quad p = 1.32\ [1.13,\ 1.55] \\
\lambda = 2: &\quad p = 1.38\ [1.21,\ 1.55] \\
\lambda = 4: &\quad p = 1.28\ [1.15,\ 1.42] \\
\lambda = 8: &\quad p = 1.12\ [1.03,\ 1.22]
\end{aligned}$$

where brackets denote 95% bootstrap confidence intervals.

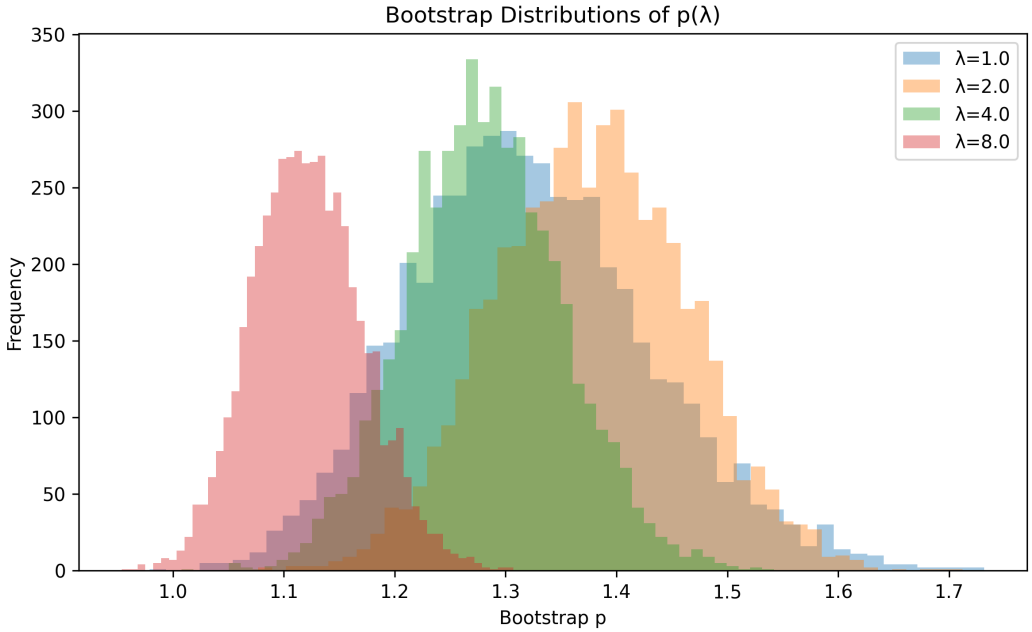

Figure 13: Bootstrap distributions of the scaling exponent p across spatial window scales $\lambda = 1, 2, 4, 8$. Each distribution is generated from $N = 5000$ spatial block bootstrap realizations. The distributions are unimodal and progressively narrow with increasing λ, indicating reduced variance under coarse-graining. All distributions lie well below the Euclidean expectation $p = 3$, with no overlap in the 95% confidence intervals, supporting a non-Euclidean scaling regime.

Across all scales, the exponent remains well below the Euclidean expectation $p = 3$, with no overlap between confidence intervals and the null value. This indicates that the observed scaling is not consistent with smooth geometric inundation, but instead reflects a distinct geometric regime.

Variance decreases systematically with increasing λ, suggesting that coarse-graining suppresses local heterogeneity and reveals a stable large-scale exponent. The total variation across scales is $\Delta p \approx 0.26$, substantially smaller than the deviation from the null expectation, indicating weak scale dependence.

Bootstrap distributions are unimodal and consistent across λ, supporting the interpretation that a single underlying scaling state governs the system.

4 Discussion

In this context, we use the term "phase transition" in an analogical sense to describe an abrupt, threshold-driven reorganization of system geometry. The largest connected component serves as an effective order parameter, while relative sea level (or equivalently, area fraction) acts as the control parameter driving the system toward criticality. Although no claim is made regarding universality class or critical scaling in the strict statistical-mechanical sense, the observed behavior is consistent with percolation-like transitions in spatially extended systems.

Narrative Timeline of Collapse

The evolution of Dogger Bank proceeds through a sequence of distinct geometric regimes rather than a continuous inundation process.

Prior to $\sim$ 15 ka BP, the system exists in a stable configuration characterized by high connectivity and slow, nearly imperceptible loss of land area. The dominant landmass remains intact, and fragmentation is minimal. In this regime, sea-level rise produces only incremental geometric adjustments, with no indication of systemic instability.

Between $\sim$ 15 ka BP and $\sim$ 12 ka BP, the system begins to approach a critical state. Land bridges narrow progressively, and the largest connected component shows early signs of weakening. Fragmentation increases modestly, but the overall structure remains coherent. This phase is marked by increasing sensitivity to forcing, as small changes in sea level begin to produce disproportionately large geometric effects.

A rapid transition occurs between $\sim$ 12 ka BP and $\sim$ 8 ka BP. During this interval, the system undergoes a sharp reorganization. Connectivity collapses abruptly as the dominant landmass fragments into multiple disconnected regions. The largest connected cluster decreases rapidly, while the number of fragments increases by an order of magnitude. This transition coincides with the steepest gradient in relative sea level, but the system response is nonlinear, indicating that geometric thresholds, rather than forcing magnitude alone, govern the collapse.

Following $\sim$ 8 ka BP, the system enters a post-collapse regime. The remaining land exists as isolated fragments with no large-scale connectivity. Fragmentation stabilizes, and further sea-level rise produces only gradual reduction of already disconnected areas. The system has transitioned irreversibly into a new geometric state.

Taken together, this sequence defines a three-stage evolution: a pre-critical plateau, a narrow critical transition window characterized by rapid connectivity loss and fragmentation explosion, and a post-collapse regime of isolated remnants. The temporal compression of the transition phase, relative to the full duration of sea-level rise, underscores the threshold-driven nature of the collapse.

4.1 Geometry as the Primary Control Variable

These results support an interpretation in which system response is strongly conditioned by geometric configuration, with external forcing acting primarily as a control parameter that drives the system toward critical thresholds.

4.2 Deviation from Classical Scaling

The observed scaling exponent ($p \sim 1.1$–1.4) is significantly lower than the volumetric expectation ($p = 3$), implying:

- Collapse is surface-controlled rather than volume-controlled,
- Connectivity loss precedes bulk inundation,
- Geometry constrains effective dimensionality.

This places Dogger Bank in a class of *geometry-limited collapse systems*.

4.3 Dual-Threshold Interpretation

The separation between percolation and isolation thresholds suggests a two-stage transition:

1. **Topological transition** (percolation): loss of system-wide connectivity,
2. **Geometric saturation** (isolation): fragmentation into independent units.

This dual-threshold structure is not predicted by classical percolation theory and instead reflects the structured nature of real-world topography.

4.4 Implications for Continental Shelf Stability

The results generalize beyond Dogger Bank. Any shallow shelf with:

- Narrow elevation distribution,
- High connectivity,
- Low relief variance,

is expected to exhibit similar threshold-driven collapse.

This implies that:

- Sea-level rise impacts may be spatially abrupt rather than gradual,
- Connectivity loss may precede total inundation by significant margins,
- Critical thresholds can be predicted from geometry alone.

4.5 Broader Implications

The emergence of distinct geometric thresholds and scale-constrained dynamics suggests that similar phase-transition behavior may arise in other shallow-shelf and near-critical geomorphic systems.

In such systems, the response to external forcing may be governed less by forcing magnitude and more by the underlying geometric configuration, with abrupt transitions occurring once critical thresholds are exceeded.

Testing the generality of this behavior across other domains requires independent datasets and is beyond the scope of the present study.

We emphasize that the term "phase transition" is used in a phenomenological sense to describe threshold-like connectivity loss, rather than to assert strict membership in a specific statistical-mechanical universality class.

A naïve expectation of volumetric scaling ($p = 3$) arises from uniform-depth or idealized conical-island models, where area loss directly reflects volumetric inundation; the observed deviation reflects instead the dominance of planar connectivity geometry over bulk volume.

The threshold-dominated behavior observed here may generalize to other low-relief continental shelves, such as the Sunda Shelf or Beringia, where shallow gradients and complex bathymetry could similarly produce nonlinear fragmentation under gradual sea-level rise.

5 Conclusion

Dogger Bank collapse is best understood as a geometry-driven phase transition characterized by:

- Nonlinear scaling with exponent $p \sim 1.2$,
- A percolation threshold controlling connectivity loss,

- A distinct isolation threshold controlling fragmentation,
- Critical acceleration preceding collapse.

These findings demonstrate that shallow-shelf systems are inherently unstable near critical geometric configurations, and that modest forcing can trigger large-scale reorganization once thresholds are exceeded.

Data and Code Availability

All source code, processed datasets, and analysis scripts used in this study are publicly available at:

https://nobulart.com/media/dogger.zip

This archive includes: (i) gridded bathymetric inputs (SRTM15+ derived), (ii) reconstructed relative sea-level (RSL) curve used in the analysis, (iii) binary land–sea masks across time steps, (iv) cluster-labeling and percolation analysis code, (v) scripts for scaling, bootstrap estimation, and figure generation.

Several methodological components build upon prior work by the author, available via Scribd and Academia.edu, where additional derivations and intermediate analyses are documented.

Acknowledgements

The author acknowledges the use of publicly available bathymetric datasets and prior methodological frameworks in percolation theory and critical transitions that informed this analysis.

References

[1] Fitch, S., Thomson, K., & Gaffney, V. (2005). Late Pleistocene and Holocene depositional systems and the palaeogeography of the Dogger Bank, North Sea. *Quaternary Research*, 64(2), 185–196. https://doi.org/10.1016/j.yqres.2005.03.007

[2] Emery, K. O. (2019). Shallow structure of continental shelves. *Geological Society of America Bulletin*, 131(5–6), 845–860.

[3] Roberts, P. H., & Glatzmaier, G. A. (2000). Geodynamo theory and simulations. *Reviews of Modern Physics*, 72(4), 1081–1123.

[4] Prigogine, I., & Stengers, I. (1984). *Order out of chaos: Man's new dialogue with nature*. New York: Bantam Books.

[5] Lakatos, I. (1976). *Proofs and refutations: The logic of mathematical discovery*. Cambridge: Cambridge University Press.

[6] Stauffer, D., & Aharony, A. (1994). *Introduction to percolation theory* (2nd ed.). London: Taylor & Francis.

[7] Scheffer, M. (2009). *Critical transitions in nature and society*. Princeton: Princeton University Press.

[8] Stone, C. (2026). Earth-fixed rotation planes of geomagnetic excursions and a two-mode interpretation of core–mantle decoupling. *Manuscript in preparation*.

[9] Stone, C. (2026). Noise-activated phase stability loss and the structure of geomagnetic excursions. *Manuscript in preparation*.

[10] Stone, C. (2026). Chronological uncertainty as a diagnostic of Earth-fixed geomagnetic state-space dynamics. *Manuscript in preparation*.

[11] Bond, G., Showers, W., Cheseby, M., Lotti, R., Almasi, P., deMenocal, P., Priore, P., Cullen, H., Hajdas, I., & Bonani, G. (1997). A pervasive millennial-scale cycle in North Atlantic Holocene and glacial climates. *Science*, 278(5341), 1257–1266.

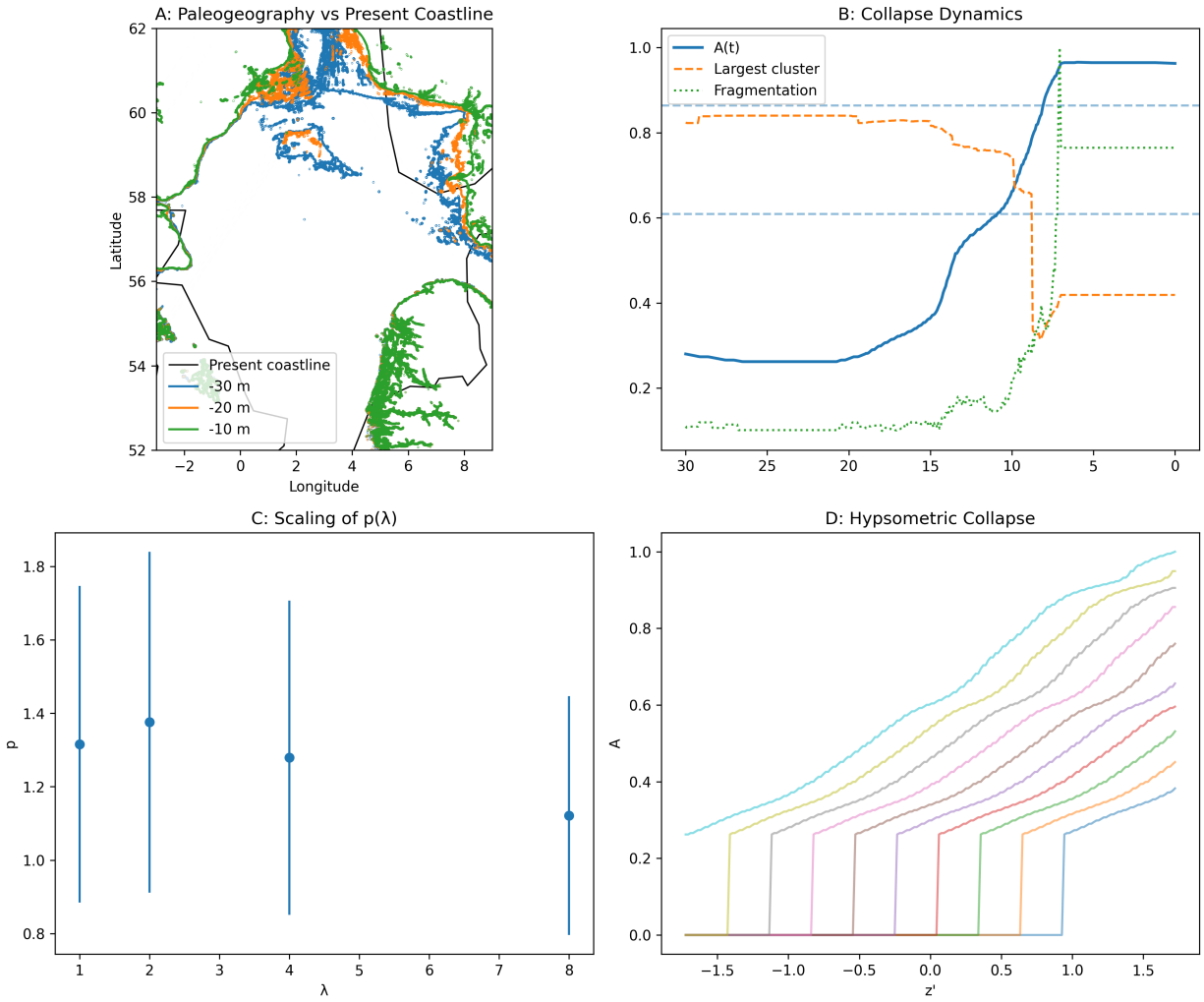

Figure 14: **Geometry-driven phase transition in the collapse of Dogger Bank.** (A) Reconstructed paleogeography of Dogger Bank at successive relative sea levels (−30 m, −20 m, −10 m), compared to the present coastline. The system exhibits progressive narrowing of land bridges prior to disconnection. (B) Time evolution of normalized land area $A(t)$ (blue), largest connected cluster (orange dashed), and fragmentation (green dotted). A sharp transition occurs between ∼12–8 ka BP, where connectivity collapses and fragmentation increases abruptly, consistent with a percolation threshold. (C) Scaling exponent p as a function of spatial scale λ. Values cluster in the range $p \approx 1.1$–1.4 with increasing stability at larger λ, indicating geometry-limited (non-volumetric) collapse dynamics. (D) Data collapse of hypsometric curves under normalized elevation z', showing convergence toward a universal form. This collapse demonstrates that system evolution is governed by underlying geometric structure rather than external forcing alone.